Mon. Not. R. Astron. Soc. **292,** 896–904 (1997)

A planet on an inclined orbit as an explanation of the warp in the β Pictoris disc

D. Mouillet,[1] J. D. Larwood,[2] J. C. B. Papaloizou[2] and A. M. Lagrange[1]

[1]*Laboratoire d'Astrophysique de l'Observatoire de Grenoble, UMR 5571, Université J. Fourier, BP 53, F-38041 Grenoble Cedex 9, France*
[2]*Astronomy Unit, School of Mathematical Sciences, Queen Mary and Westfield College, Mile End Road, London E1 4NS*

Accepted 1997 August 15. Received 1997 April 18; in original form 1996 October 2

ABSTRACT

We consider the deformation that has recently been observed in the inner part of the circumstellar disc around β Pictoris with the *HST*. Our recent ground-based, adaptive optics coronographic observations confirm that the inner disc is warped. We investigate the hypothesis that a yet undetected planet is responsible for the observed warp, through simulations of the effect of the gravitational perturbation resulting from a massive companion on the disc. The physical processes assumed in the simulations are discussed: since the observed particles do not survive collisions, the apparent disc shape is driven by the underlying collisionless parent population. The resulting possible parameters for the planet that are consistent with the observed disc deformation are reviewed.

Key words: circumstellar matter – stars: individual – β Pictoris – planetary systems.

1 INTRODUCTION

An important discovery by *IRAS* was the detection of infrared (IR) excess due to cold material around a number of main-sequence stars. Among them, β Pictoris exhibits one of the largest excesses (Aumann 1985). Shortly after the *IRAS* results, a disc of dust was imaged around this star (Smith & Terrile 1984). Since then, the disc has been extensively studied, as it is expected to be related to planetary systems, possibly in a state of evolution different from that of our Solar system.

The composition of the disc is complex. Micron-sized grains are detected through scattered light (Kalas & Jewitt 1995, and references therein; Mouillet et al. 1997) and thermal emission (Lagage & Panin 1994). The presence of small amounts of submicron grains is inferred from 10-μm spectrophotometry (Knacke et al. 1993). Larger grains (millimetre-sized) are detected through photometry at millimetre wavelengths (Chini et al. 1991; Zuckerman & Becklin 1993). Kilometre-sized bodies have also been proposed to account for the very peculiar spectroscopic variability of β Pictoris (Lagrange, Ferlet & Vidal-Madjar 1987). Gas is detected spectroscopically through the presnece of absorption lines. However, the gas-to-dust ratio is probably ≤ 1, i.e., much less than that in the environment of young stars such as T Tauri, or in star-forming regions. Most of the gas is probably confined very close to the disc (Lagrange et al. 1996, and references therein).

The total mass of the disc is very uncertain, as most of it comes from the largest bodies. About one Earth mass is necessary to account for optical to millimetre observations. If the particle size distribution follows a law of the form

$$\mathrm{d}n(a) \propto a^{-3.5}\,\mathrm{d}a,$$

with $n(a)$ being the number of particles of size greater than a, up to kilometre-sized bodies, the mass would be several tens of Earth masses (Backman & Paresce 1993).

The origin and evolution of this system is still the subject of active research, and one point of investigation is the possible presence of planets within the disc. From the theoretical point of view, planets are expected to be formed out of the circumstellar disc that accompanies the star during the process of formation. The time-scale estimated for this process (see Lin & Papaloizou 1985) is characteristically less than the estimated lifetime of β Pictoris $\sim 2 \times 10^8$ yr (Paresce 1991). Thus it is reasonable to suppose that planets have had time enough to form.

Obtaining direct evidence for the existence of planets around early-type stars such as β Pictoris is far from straightforward. Direct imaging is still beyond current observational capability because of the high contrast between the star and the planet. Photometric variations

have been observed (Lecavelier et al. 1995) which are consistent with the occultation of β Pictoris by an orbiting Jupiter-like planet. However, this has not been firmly established (observation of another occultation is needed to sweep all doubts away). Radial velocity studies, like those performed to detect giant planets around solar-type stars such as 51 Peg, 47 UMa and others (Mayor & Queloz 1995; Marcy & Butler 1996), would not provide enough accuracy to detect giant planets at distances of about a few au from these usually rapidly rotating early-type stars.

Signatures of planets can result from their gravitational effect on the disc. The observed clearing of the inner region of the disc has been attributed to the gravitational effect of an orbiting planet (Roques et al. 1994). However, other physical processes can explain the observed dust distribution as well.

The gravitational influence of a planet has been invoked in order to explain the observed high rate of cometary infall (about 1000 per year corresponding to $\sim 10^{-15}$ $M_\odot$ yr^{-1}). Beust & Morbidelli (1996) propose that mean motion resonances between the orbits of kilometre-sized bodies and a planet in a longer-period eccentric orbit can produce the right quantity and orbits of infalling bodies. They predict long-term variabilities, which are currently being tested via a spectroscopic survey. Such a model requires a steady flux of kilometre-sized bodies from the outer to inner regions of the disc to occur as a consequence of collisions.

Finally, observations with the *Hubble Space Telescope* (*HST*) provide high signal-to-noise (S/N) data on the light scattered from the inner part of the disc down to 25 au from the star (Burrows, Krist & Stapelfeldt 1995). They reveal a slight inclination ($\sim 3°$) of the inner disc mid-plane up to about 50 au, to the outer disc mid-plane. Burrows et al. (1995) proposed that a planet on an orbit inclined to the outer disc plane might be the most probable explanation for these observations. In Section 2 we show recent ground-based observations imaging the same region of the disc for comparison. In Section 3 we review the physical properties of the disc, to determine how a hypothetical planet would act on it. This leads to 3D numerical simulations of the simultaneous behaviour of large numbers of test particles representing a disc population of kilometre-sized objects under the gravitational field of the star and a massive companion on an inclined, and possibly eccentric, orbit. In Section 4 we present the results. Finally, we discuss the possible parameters for the companion consistent with its presence being able to explain the brightness asymmetry of the inner β Pictoris disc (Section 5), and present our conclusions (Section 6).

2 OBSERVED ASYMMETRY OF THE INNER PART OF THE β PICTORIS DISC

2.1 Adaptive optics observations of the inner disc

No warp has been detected in the classical coronographic observations outside 80 au. In order to observe the disc closer to the star, one needs high-angular-resolution observations, i.e., either space observations or images corrected for atmospheric effects. Recently, adaptive optics coronographic images of the β Pictoris disc enabled us to detect the disc in the near-infrared (NIR) through scattered light down to about 25 au from the star (Mouillet et al. 1997). Similar resolution was obtained with the *HST* in the optical range (Burrows et al. 1995).

We performed new observations of the β Pictoris disc with a coronograph coupled to the ESO adaptive optics system ADONIS on 1996 January 5 in the *J* band (Fig. 1). The inner region (20–80 au) is observed with an angular resolution similar to that of the *HST*. However, the correction for atmospheric turbulence makes it more difficult to subtract perfectly the stellar light which remains after the mask, so that some residuals of the point-spread function (PSF) temporal variations remain on the image. Details of the observing method and of the reduction procedure can be found in Beuzit, Mouillet & Lagrange (1997).

From Fig. 2 we see that the intensity peak lies on one of two lines according to whether it is nearer or further than 50 au from the centre. Thus the disc mid-plane inside 50 au is inclined at about 3° to the outer disc mid-plane. The effect of the warp is hardly seen, but none the less it is consistent with the *HST* data in terms of amplitude and extent.

These observations confirm previous results (Burrows et al. 1995; Mouillet et al. 1997): the surface brightness profile $I(r)$, which is measured to be very steep far from the star (Kalas & Jewitt 1995), becomes flatter as the distance to the star, r, decreases from 100 au down to 25 au. For $r > 100$ au, $I(r) \propto r^{-3.5}$. For $50 < r < 100$ au, $I(r) \propto r^{-1.3}$. For $r < 50$ au, the profile is even flatter (Fig. 3). Consequently, the form of the optical depth as a function of r, given by $\tau(r) = 5 \times 10^{-3}\ (r/100)^{-1.7}$, which is valid for $r > 100$ au, cannot be used for smaller values of r. The inferred form depends on the precise model involving a combination of thermal IR and scattering observations, but it converges on a progressive flattening up to a maximum value of 10^{-3}–10^{-2} at around $r = 40$ au, thereafter decreasing inwards. Very little residual dust is expected closer than 15 au, since it would induce IR excesses in the NIR which are not observed.

2.2 The planetary hypothesis

The deformation of the inner disc mid-plane relative to the outer disc mid-plane is not the only asymmetry observed in the β Pictoris disc (Lagage & Pantin 1994; Kalas & Jewitt 1995). All these asymmetries are difficult to explain in the context of a low-mass disc consisting of many small objects under a dominant potential arising from a central point mass, since any azimuthal inhomogeneities would be expected to disappear on an orbital time-scale (a few 1000 yr at 100 au). A single physical process is unlikely to be responsible for all of them, since very different spatial scales are involved together with different geometries. For instance, anisotropic scattering properties, together with a slightly inclined disc, were proposed to explain the so-called 'butterfly' asymmetry (the mid-plane is not an axis of symmetry of the brightness distribution; Kalas & Jewitt 1995). However, such an explanation is unable to account for any radial-dependent asymmetry. Another idea is that the local production of very small grains as collision products followed by their efficient acceleration by radiation pressure could produce catastrophic blow-out in some random part of the disc (Artymowicz 1996). Such a mechanism could explain any kind of asymmetry without the need for a planet. However, the strong asymmetry (global azimuthal

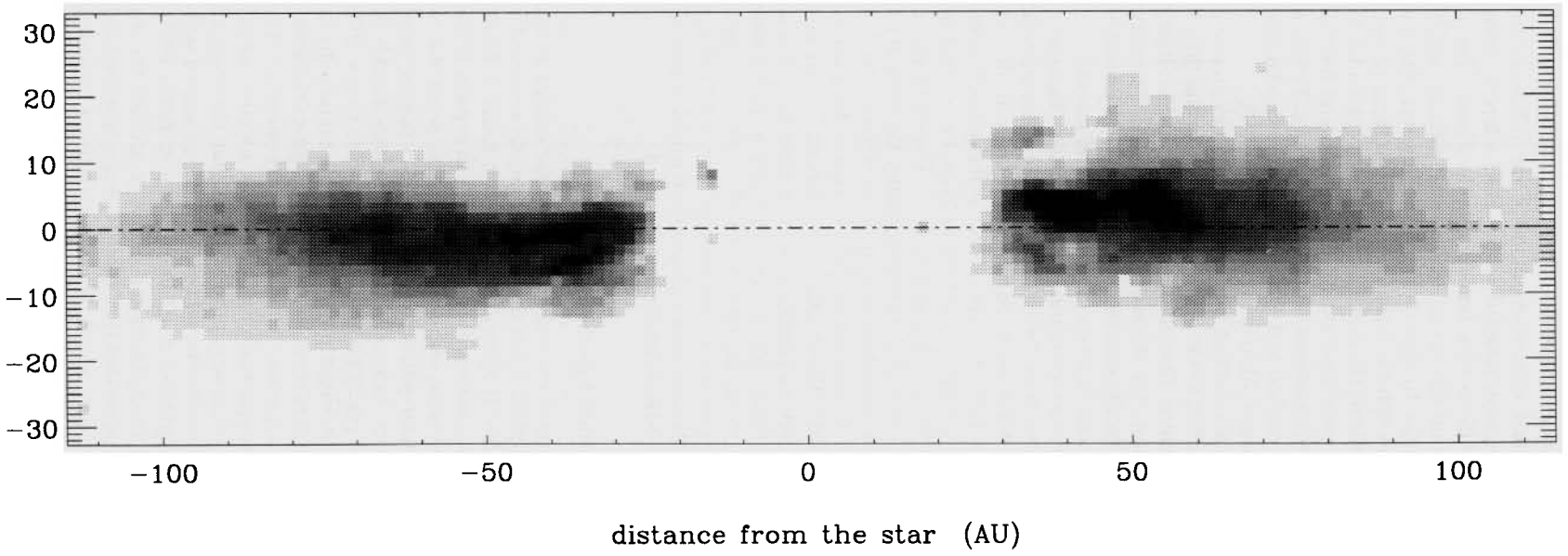

Figure 1. Adaptive optics observations in the J band of the inner disc of β Pictoris, 1996 January 5. The axes are marked in au. Inward of 50 au, the disc mid-plane is inclined with respect to the outer disc mid-plane (dashed line).

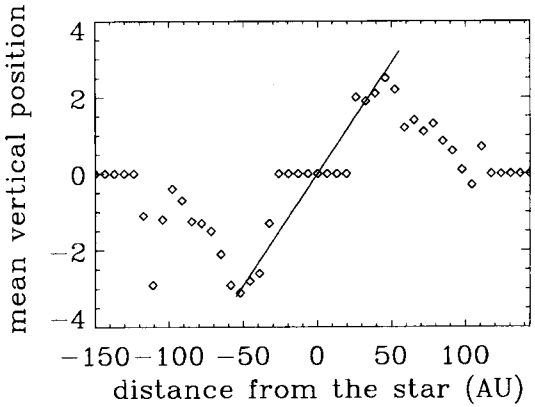

Figure 2. The observed vertical deformation of the disc above the outer disc mid-plane. The axes are marked in au. The vertical deformation is measured from the centroid of the brightness distribution in the direction normal to the outer disc mid-plane. The value zero is adopted when the measurement is not possible (closer than 25 au and further than 110 au). The solid line is the linear fit for the inner part. We define the extent of the deformation as the distance at which the slope of the fit starts to decrease. The extent of the deformation is 50 au, and the corresponding inclination 3°.

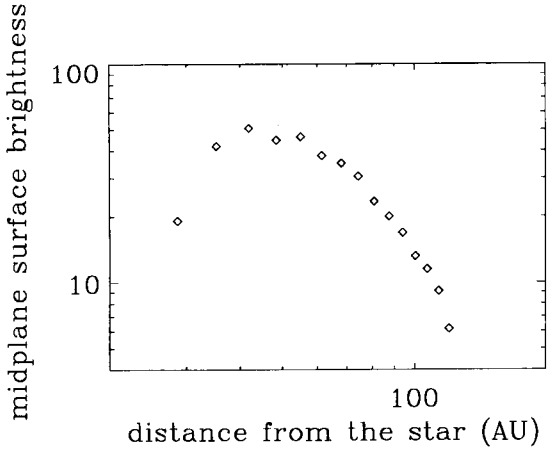

Figure 3. Mid-plane surface brightness of the disc.

structure) of the observed warping with respect to the central star makes this an implausible explanation for it. In this paper we investigate the possibility that the warping asymmetry is produced by an as yet undetected planet, in order to see what constraints might be put on its parameters. Although we are not able to claim this as a unique explanation, we are able to show that the required parameters are reasonable and not at present in conflict with constraints arising from the lack of observational detection through either imaging or spectroscopy.

3 NUMERICAL SIMULATIONS OF THE INFLUENCE OF A PLANET

3.1 Physical processes in the β Pictoris disc

The dynamics in the disc is dominated by the gravitational force of the central star, to which may be added effects due to any possible perturbing planets. The mass of observed disc material is negligible. Radiation pressure is important for small grains less than a characteristic size $a_c = 2$ μm (Artymowicz 1988). For such grains the force due to radiation pressure exceeds gravity, so that they are on unbound hyperbolic orbits. Accordingly, their lifetime is of the order of the crossing time of the disc and thus very short. The Poynting–Robertson effect is negligible, as is gas drag due to the small quantity of gas present (Artymowicz 1995).

The main quantity determining the grain collision frequency is the optical depth of the dust, τ. The mean time between collisions is given by

$$t_c = \frac{P_{ORB}}{\pi\tau},$$

where P_{ORB} is the local orbital period. For the β Pictoris disc, the optical depth has been estimated to be typically 5×10^{-3} for small size scattering particles. Supposing that the particle size distribution is given by $dn(a) \propto a^{-3.5}\, da$ (which might arise from collision processes), the smallest μm-sized grains contribute most of the optical depth. The collision time at 100 au is then typically 10^5 yr for such grains. The characteristic impact velocities are $\sim v_r = i v_{orb} \sim 1$ km s^{-1}, where v_{orb} is the orbital velocity, and i is a characteristic inclination in radians associated with a grain orbit. The expected impact velocities are sufficient to destroy the colliding particles. The lifetime of the smallest particles in bound orbits is therefore of the order of the collision time ($\sim 10^5$ yr at 100 au and even shorter closer than 100 au), and in any case much less than the age of the system. Thus they need to be replenished by the destruction of larger particles. For normal solid-state densities, the surface density of disc material contained in small particles is $\Sigma \sim a_c \tau$, which implies a mass of $\sim 10^{-9}\, M_\odot$ contained within 100 au, and a mass-loss rate of around $10^{-4}\, M_\odot$ yr^{-1}.

Assuming that collisions will determine both the particle size distribution through fragmentation processes [$dn(a) \propto a^{-3.5}\, da$] and the particle lifetimes, most of the mass in the system will reside in the largest bodies which also contribute least to the optical depth. It is natural to regard the larger bodies as a primary source of material to drive the global mass-loss rate of the system. After a (destructive) collision, the particle ejection velocities, as viewed in the centre-of-mass frame, are negligible compared to the orbital velocity of the parent particles. Consequently, the global distribution of particles of any given size is not driven by interaction processes, but is closely related to that of the much bigger parent bodies. This means that the disc shape of the small particles detected in scattered light is driven by the kinematic effect of gravitation on long-lived (as old as the system) particles.

Because of the detection of this disc, the collision time of the largest bodies is expected to be greater than the age of the system. As an illustrative example, if the largest bodies are kilometre-sized, the given size distribution indicates that $\sim 3 \times 10^{-5}\, M_\odot$ should be contained in these bodies, and the characteristic collision time between them should be $\sim 3 \times 10^9$ yr. If a significant amount of the material involved in collisions ends up in small particles, then the supply rate could be as much as $\sim 10^{-14}\, M_\odot$ yr^{-1}. Note, too, that collisions between the kilometre-sized bodies also result in an inward radial migration of the distribution, much as for viscous accretion discs or planetary rings. The effective diffusion coefficient is $D_c \sim H^2/t_c$, H being the vertical thickness, and t_c being the collision time. For $H = 0.1r$, and $t_c = 10^9$ yr, this gives a diffusion time-scale of $r^2/D_c \sim 10^{11}$ yr, corresponding to a mass-flow rate of $\sim 3 \times 10^{-16}\, M_\odot$ yr^{-1}. Apart from lifetime considerations, a large number of such kilometre-sized bodies is expected in the β Pictoris disc to explain the spectroscopic detection of highly redshifted variable gas close to the star (Beust et al. 1996). Were even larger bodies to exist around the star, like the kilometre-sized objects, they might also provide a source of small particles, but they would be expected to have a similar or perhaps even longer effective collision frequency, and thus behave in a similar way from the point of view of our analysis.

Accordingly, we model the disc as a system containing a large number of long-lived objects, which, as far as the majority are concerned, are collisionless. We then suppose that, as they do not survive more than one collision, the small particles reflect the distribution of the large bodies. We are thus concerned with kinematic patterns produced by non-interacting particles.

3.2 Numerical simulations

The numerical simulations are based on a collisionless adaptation of the smoothed particle hydrodynamics (SPH) code described in Larwood & Papaloizou (1997, and references therein). In this version, pressure and viscous forces are removed, so that we consider a purely kinematic model. The code follows the velocity and position coordinates of typically 15 000 particles over thousands of revolutions of the perturbing companion. The particles were initially set up in circular motion in a disc configuration with aspect ratio $H/r = 0.1$. They were inserted, using a random number generator, according to the following Σ distribution (in model units) to represent schematically the matter distribution in the β Pictoris disc [since the particles are collisionless, the precise form of $\Sigma(r)$ has no effect on the amplitude and extension of the consequent warp]:

for $1.2 \le r \le 4.2$, $\quad \Sigma(r) \propto r^{-0.5}$,

for $4.2 \le r \le 6$, $\quad \Sigma(r) \propto r^{-1.5}$.

Table 1. Parameter sets of the simulations in model units (see text).

Model	M/M_*	D	e	i	Run time
01	1e-3	1.	0.	3	1e5
02	4e-3	0.5	0.	3	1e5
03	9e-3	0.33	0.	3	3e5
04	5e-3	1.	0.	3	1e5
05	1e-2	0.7	0.	3	1e5
06	1e-2	1.	0.	3	1e5
07	1e-3	0.7	0.1	3	7.5e5
08	1e-3	0.7	0.3	3	3e5
09	1e-3	0.7	0.5	3	3e5
10	1e-2	0.7	0.1	3	3e5
11	1e-2	0.7	0.3	3	3e5
12	1e-2	0.7	0.5	3	3e5
12b	1e-2	0.7	0.5	6	3e5

The model unit of length corresponding to $r-1$, $R_{\rm unit}$, is arbitrary, whereas the corresponding unit of time, $t_{\rm unit}$, is the inverse orbital frequency at $R_{\rm unit}$.

The companion is initiated in a generally eccentric orbit such that, in a Cartesian coordinate system with origin at the centre of mass, and (x, y) plane coinciding with the initial disc mid-plane, both the planet and the line of nodes are on the x axis at time $t=0$. Parameters associated with the simulations are the mass ratio of the planet and central star, M/M_*, the semimajor axis, D, the eccentricity, e, and the inclination of the planet's orbit, i, to the disc mid-plane. Finally, the run time since initiation with the orbital configuration as described above is also an important parameter, as this determines the extent of the warped deformation. Table 1 gives the chosen parameters for various simulations. In order to compare the simulation results with observation, we have derived the apparent surface brightness distribution associated with the simulation particles, that is the integration along a line of sight of the scattered stellar flux from each particle (Fig. 4). We note that a companion in an inclined orbit breaks the azimuthal symmetry of the system. The orientation of the line of sight to line of nodes is unknown in the case of β Pictoris, and

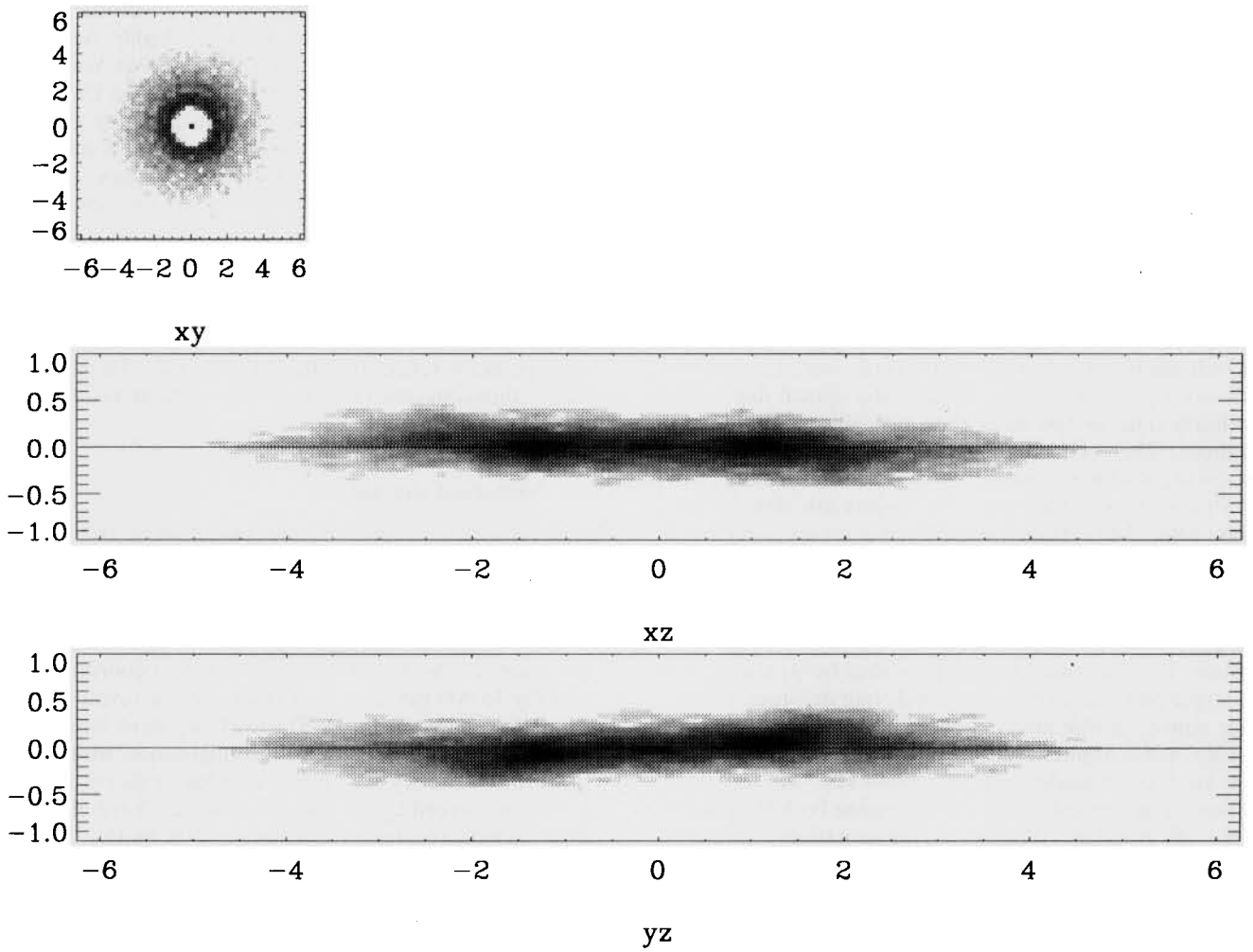

Figure 4. Apparent surface brightness distribution associated with the simulation particles. The represented data set is model 05 at run time = 10^5. For each projection plane, the axes are scaled in model units.

should be considered as a free parameter in fitting the observations.

4 RESULTS

4.1 Simple description of the effect of a companion on the vertical elevation of the disc

Adopting the cylindrical coordinates (r, φ, z), equivalent to our Cartesian system, the vertical elevation of a razor-thin disc moving under the influence of a companion in an inclined circular orbit with small i satisfies

$$\frac{d^2z}{dt^2} + \Omega_z^2 z = \frac{3}{4}\frac{GMD^2}{r^4}\sin(2i)\sin(\varphi). \quad (1)$$

Here Ω_z is the frequency of vertical oscillations, and the term on the right-hand side is the secular vertical acceleration due to the companion. This has been expanded to lowest order in D/r, which becomes an increasingly accurate procedure further out in the disc (Larwood & Papaloizou 1997). The precession frequency, $\omega_p = \Omega - \Omega_z$, is such that $|\omega_p| \ll \Omega$, where Ω is the angular velocity. For particles in nearly circular orbits, $\varphi = \Omega t = \text{constant}$, and for small e and i,

$$\omega_p = -\frac{3}{4}\frac{GMD^2}{\Omega r^5}.$$

Using the above in (1), we obtain the approximate solution with zero elevation at $t = 0$,

$$z = -\frac{3}{8}\frac{GMD^2\sin(2i)}{\Omega\omega_p r^4}[\sin(\varphi) - \sin(\varphi - \omega_p t)]. \quad (2)$$

In this purely kinematic model, the inclined orbit of the companion breaks the mid-plane symmetry and forces the test particle orbits to precess around the orbital angular momentum axis of the companion. If phase mixing due to the r-dependence of ω_p is complete ($|\omega_p t| \gg 1$), this process thickens the disc so that the aspect ratio appears to be equal to the orbital inclination. The vertical amplitude of the deformation is thus directly related to the inclination of the companion's orbit.

This relation is verified numerically for the simulation data (Fig. 5). In addition, we note that the apparent amplitude of the warp depends on the orientation of the line of sight (Fig. 6). The observability of the warp is maximized when it (assumed to lie in the outer disc mid-plane) is at about 30° to the line of nodes.

4.2 Radial extent of the deformation

A deformation corresponding to a thickened disc is established very quickly close to the star and then propagates outwards. As indicated above by (2), the location of the end of the deformation corresponds very roughly to the place where the inverse precession frequency is roughly equal to the run time ($|\omega_p t| \sim 1$). Note, however, that this will overestimate the location of the edge of the deformation, because many precession periods are needed to ensure enough phase mixing for the full deformation to be produced. Nevertheless, the number of precession periods required should not depend on radius, so that we expect the scaling relation

$$r \propto (MD^2 t)^{2/7}.$$

This form occurs because the propagation rate is driven by the tidal force, which is proportional to MD^2.

The radial dependence of the precession frequency, namely

$$\omega_p \propto MD^2 r^{-7/2},$$

has been checked in the simulations (Fig. 7).

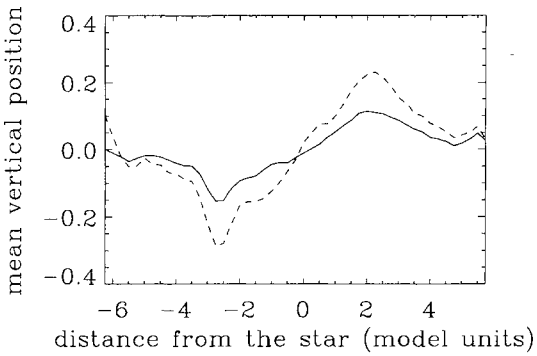

Figure 5. Linear dependence of the amplitude of the warp on the inclination of the orbit of the companion. The axes are scaled in model units. The amplitude of the warp is quantified in the same way as for observational data (see Fig. 2). The effect is twice as large for an inclination of 6° (dashed line, from model 12b), compared with an inclination of 3° (solid line, from model 12), all other parameters being equal.

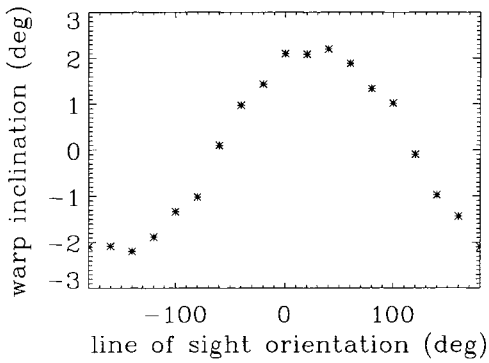

Figure 6. Observability of a warp as a function of the line of sight orientation. The x axis gives the orientation of the assumed line of sight to line of nodes. The y axis gives the corresponding apparent inclination of the warp in simulated data (with a 3° inclined companion orbit), measured in the same way as for the observational data (Fig. 2).

4.3 Companion eccentricity and particle inflow towards the star

We now explore the consequence of a possible eccentricity of the companion orbit. Increasing eccentricities induce very little direct observable effect for a disc seen edge-on (Figs 8 and 9). Consequently, this value is poorly constrained by the observations of the β Pictoris disc. Yet the azimuthal distribution of particles is affected, with the for-

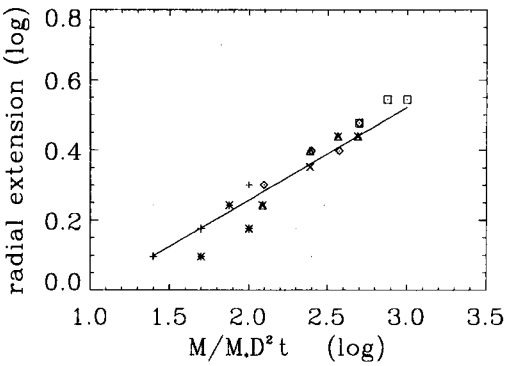

Figure 7. Radial extent of the deformation. The extent of the warp (in model units) is measured in the same way as for the observational data (Fig. 2). It is displayed versus MD^2t in a log–log plot. The simulation data comes from zero-eccentricity models (model 01: +, model 02: ★, model 04: ◇, model 05: △, model 06: □) and a line-of-sight orientation of 60° (where the warp observability is umambiguous). Similar results are obtained with other models and orientations. The best-fitting power-law index is numerically measured to be 0.29, in good agreement with the theoretical expectation (2/7).

mation of spiral-like features. The stronger the eccentricity, the sharper such features become.

We also notice that the eccentricity of some disc particles is increased to high values, with the result that they are thrown towards the star and end up inside the companion's orbit. Out of the initial number of 15 354 particles with $r > 1.2$, a few go inside the companion's orbit ($D = 0.7$) in model 11 ($e = 0.3$), as do a few dozen in model 12 ($e = 0.5$).

5 POSSIBLE PARAMETERS FOR THE PERTURBER

The comparison between the simulation results and observations allows derivation of possible parameters for the companion orbit. First, the observed inclination of 3° requires an orbit inclination of 3°–5° to the outer disc midplane, depending on the angle between the line of sight and the line of nodes (these are assumed to be coplanar). This angle is poorly constrained, but should not lie in the [−80°, −50°] (modulo 180°) range, so that the deformation is observable.

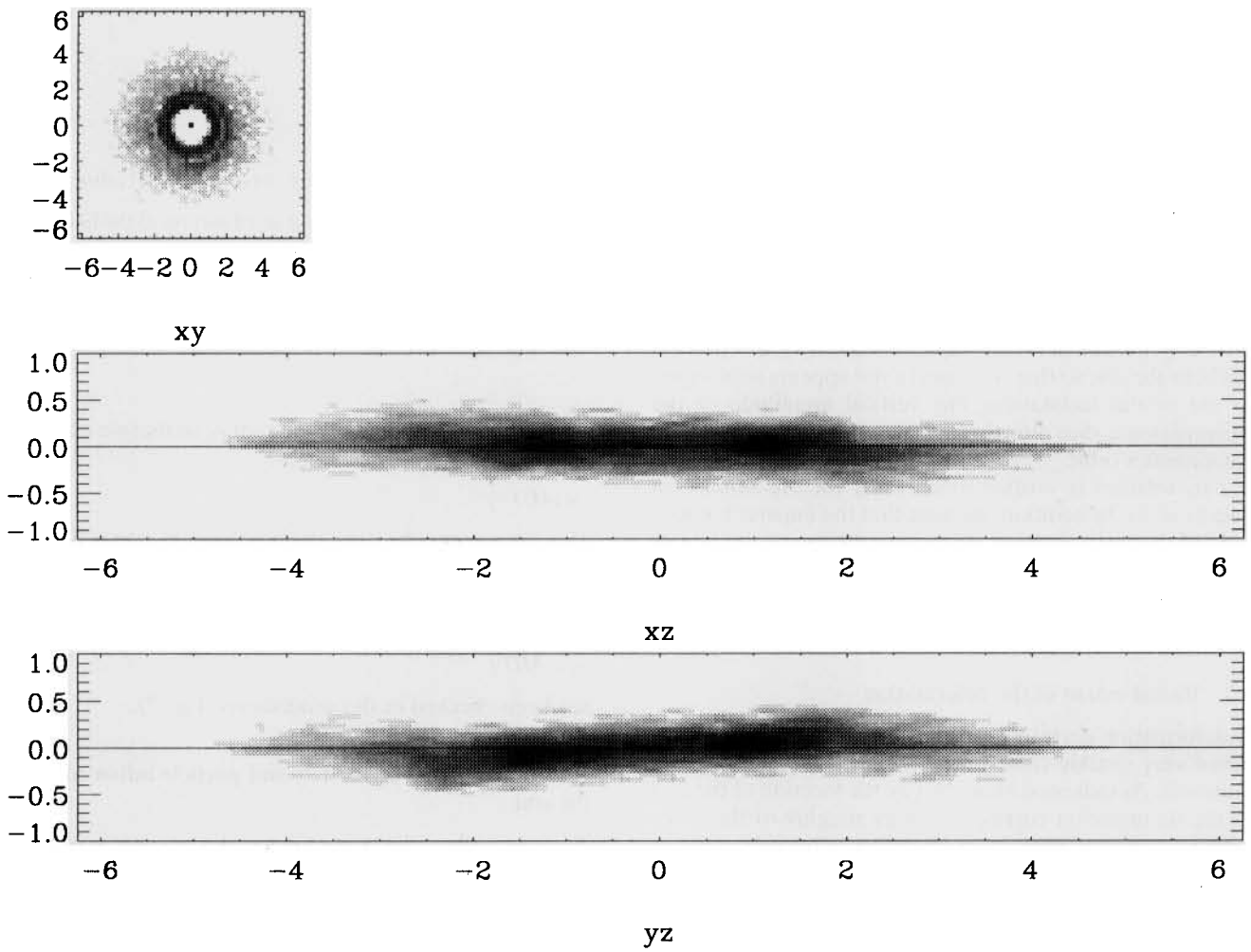

Figure 8. Same as Fig. 4, for model 10 at run time = 3×10^5; the companion orbit eccentricity is 0.1.

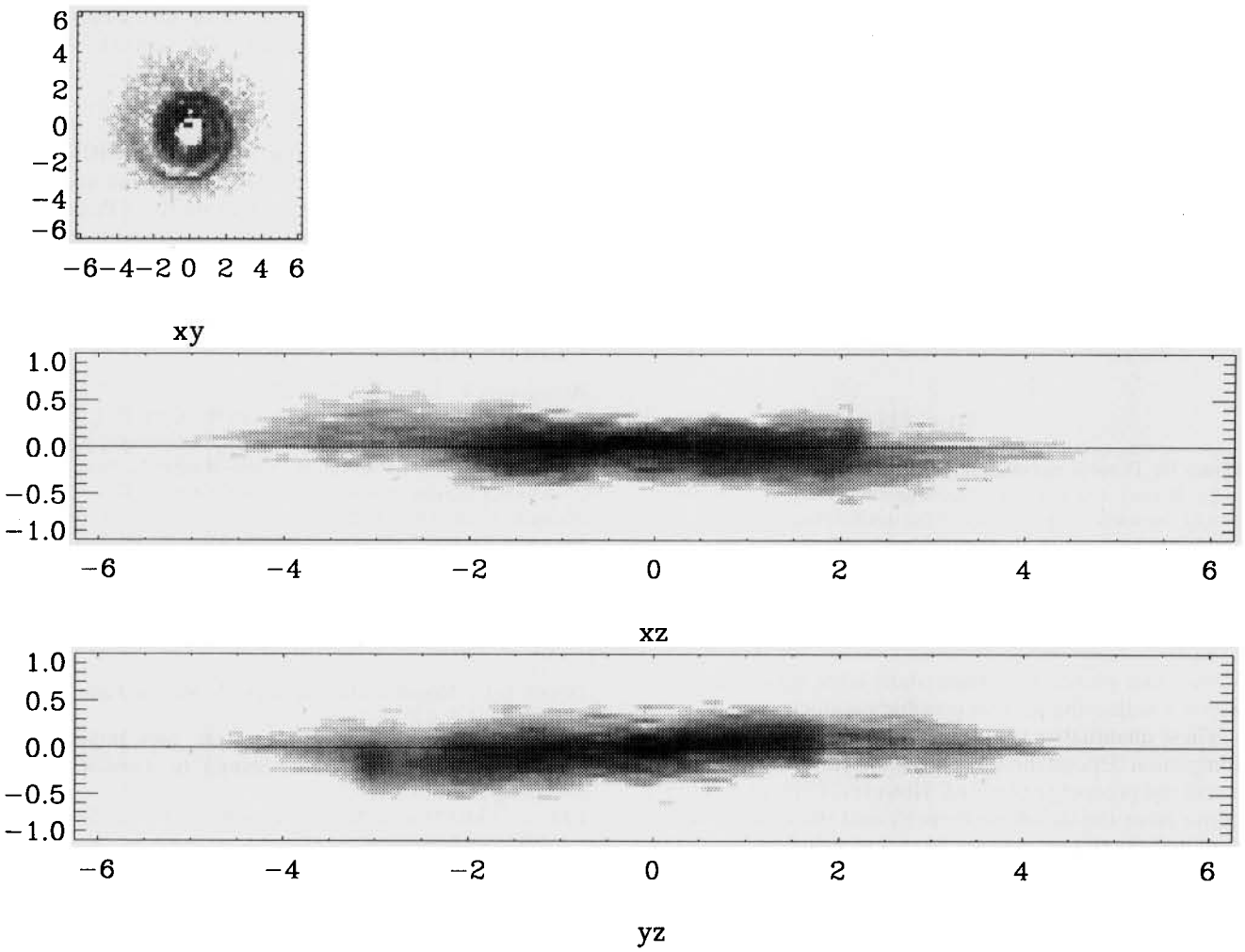

Figure 9. Same as Fig. 4, for model 12 at run time $=3\times10^5$; the companion orbit eccentricity is 0.5.

Secondly, the companion orbit is not well constrained by the observation of an edge-on disc, so that it can be considered as a free parameter in the simulations. This could have an important role in feeding material into the inner disc. This, taken together with the general inward migration of the kilometre-sized bodies, may be related to the cometary infalls observed via spectroscopy, at the rate of about 1000 kilometre-sized bodies per year. Gravitational perturbations are likely to be involved in these processes. A massive companion invoked to explain the imaging data could then also provide at least part of an explanation for these infalls, as long as its eccentricity is significantly larger than 0.1. We also remark that a moderately large eccentricity is required if an eccentricity pumping mechanism, through mean motion resonances, is supposed to work on particle orbits interior to the planet.

Finally, observations show a radial extension of the warp of 50 au. If we arbitrarily choose the model unit $R_{\rm unit}=10$ au, then the corresponding model time unit is

$$t_{\rm unit}=\left(\frac{r^3}{GM_*}\right)^{1/2}=5.2\ \text{yr}.$$

According to the simulations (Fig. 7), the observed extent of the warp [$\log(R/R_{\rm unit})=0.7$] then requires the condition

$$\frac{M}{M_*}\left(\frac{D}{R_{\rm unit}}\right)^2\frac{t}{t_{\rm unit}}\sim3000.$$

Assuming that the companion formation is rapid, so that the propagation time of the warp is close to the age of the system, $t\sim2\times10^8$ yr. Then a planet with $MD^2=10^{-4}M_*$ (10 au)^2 can account for the observed warp (Fig. 10). In the framework of these simulations, the orbit of the companion is interior to the observed disc, so that $D\leq20$ au. The absence of radial velocity variations larger than about 1 km s^{-1} in our spectroscopic data gathered since 1984 implies that $M^2/D_{\rm au}\leq5\times10^{-4}$. Meanwhile, the indirect detection of any nearby companion does not constrain further the range of possible parameters. Finally, the possible parameters define a giant planet with a mass $10^{-5}\leq M/M_*\leq10^{-2}$, located at a corresponding respective distance from the star $20\leq D\leq1$ au. Such a planet may be detected in photometry if it crosses the line of sight, which requires that the Earth is in the plane of the planet's orbit to within a precision of $0\overset{\circ}{.}06/D_{\rm au}$. Actually, Lecavelier et al. (1995) propose a

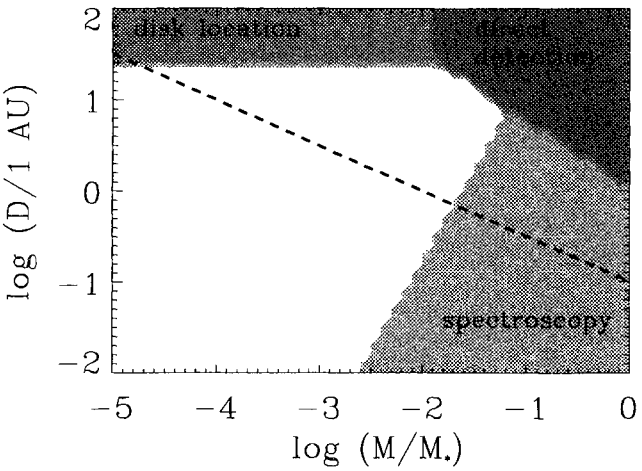

Figure 10. Possible parameters M and D for the gravitational perturber in a log–log diagram. The constraint derived from the extension of the warp is represented by the dashed line. Shaded regions are forbidden because of observational constraints (see text) and the assumption that the companion orbit is inside the disc.

Jupiter-like planet to explain short-term light variations, which is within the present possible parameter range.

These quantitative results on the possible parameters of a companion depend directly on the system lifetime, t, which is still not precisely estimated. However, Crifo et al. (1997) derive from the stellar photometry and the new *Hipparcos* data that the system may not be younger than 10^7 yr. In this case, our corresponding constraint would shift to $MD^2 = 2 \times 10^{-3} M_*$ (10 au)^2. This would restrict the possible parameters to more massive companions ($10^{-3.5} \leq M/M_* \leq 10^{-2}$) between 20 and 3 au.

6 CONCLUSIONS

From visible as well as NIR imaging observations, the disc around β Pictoris is detected through scattered light from micron-sized grains. These grains are short-lived because of destructive collisions and the action of radiation pressure. Assuming that their distribution is the same as an underlying parent population of kilometre-sized bodies, the apparent distribution of matter within the disc can be derived from numerical simulations of collisionless particles. Such simulations are able to reproduce the observed warp in the inner part of the disc as a result of the effect of gravitational perturbations due to a planet in an orbit inclined at 3°–5° to the outer disc mid-plane. Such a planet should be located between 1 and 20 au, with a corresponding mass, respectively, between $10^{-2} M_*$ and $10^{-5} M_*$.

ACKNOWLEDGMENTS

This work was supported in part by EU grant ERB-CBRX-CT93-0329. We are grateful to Alain Lecavelier and Alfred Vidal-Madjar for fruitful discussions on the β Pictoris disc, and to N. Hubin and the ESO staff in La Silla for their help in the preparation and making of the ADONIS observations.

REFERENCES

Artymowicz P., 1988, ApJ, 335, L79
Artymowicz P., 1996, in Siebenmorgan R., Kaufi H. U., eds, The Role of Dust in the Formation of Stars. Springer, p. 137
Artymowicz P., 1995, in Ferlet R., Vidal-Madjar A., Proc. 10th IAP Conf., Editions Frontières, Gif-sur-Yvette, p. 47
Aumann H. H., 1985, PASP, 97, 885
Backman D. E., Paresce F., 1993, in Levy E. H., Lunine J. I., Matthews M. S., eds, Protostars and Planets III. Univ. Arizona Press, p. 1253
Beust H., Morbidelli A., 1996, Icarus, 120, 358
Buest H., Lagrange A.-M., Plazy F., Mouillet D., 1996, A&A, 310, 181
Beuzit J.-L., Mouillet D., Lagrange A.-M., Paufique J., 1997, A&AS, 125, 175
Burrows C. J., Krist J. E., Stapelfeldt K. R., 1995, BAAS, 187, 32
Chini R., Kruegel E., Kreysa E., Shustov B., Tutukov A., 1991, A&A, 252, 220
Crifo F., Vidal-Madjar A., Lallement R., Ferlet R., Gerbaldi M., 1997, A&A, in press
Kalas P., Jewitt D., 1995, AJ, 110, 794
Knacke R. F. et al., 1993, ApJ, 418, 440
Lagage P. O., Pantin E., 1994, Nat, 369, 628
Lagrange A.-M., Ferlet R., Vidal-Madjar A., 1987, A&A, 173, 289
Lagrange A.-M. et al., 1996, A&A, 310, 547
Larwood J. D., Papaloizou J. C. B., 1997, MNRAS, 285, 288
Lecavelier A., Deleuil M., Vidal-Madjar A., Ferlet R., Nitschelm C., Nicolet B., Lagrange A.-M., 1995, A&A, 299, 557
Lin D. N. C., Papaloizou J. C. B., 1985, in Black D. C., Matthews M. S., eds, Protostars and Planets II. Univ. Arizona Press, p. 981
Marcy G. W., Butler R. P., 1996, ApJ, 464, L147
Mayor M., Queloz D., 1995, Nat, 378, 355
Mouillet D., Lagrange A. M., Beuzit J. L., Renaud N., 1997, A&A, 324, 1083
Paresce F., 1991, A&A, 247, L25
Roques F., Scholl H., Sicardy B., Smith B. A., 1994, Icarus, 108, 37
Smith B. A., Terrile R. J., 1984, Sci, 226, 1421
Zuckerman B., Becklin E. E., 1993, ApJ, 414, 793